Modelling earth current precursors in earthquake prediction

Domenico Patella ([1]), **Antonio Tramacere** ([2]) **and Rosa Di Maio** ([1])
([1]) *Dipartimento di Geofisica e Vulcanologia, Università di Napoli «Federico II», Napoli, Italy*
([2]) *Dipartimento di Geologia e Geofisica, Università di Bari, Italy*

Abstract
This paper deals with the theory of earth current precursors of earthquake. A dilatancy-diffusion-polarization model is proposed to explain the anomalies of the electric potential, which are observed on the ground surface prior to some earthquakes. The electric polarization is believed to be the electrokinetic effect due to the invasion of fluids into new pores, which are opened inside a stressed-dilated rock body. The time and space variation of the distribution of the electric potential in a layered earth as well as in a faulted half-space is studied in detail. It results that the surface response depends on the underground conductivity distribution and on the relative disposition of the measuring dipole with respect to the buried bipole source. A field procedure based on the use of an areal layout of the recording sites is proposed, in order to obtain the most complete information on the time and space evolution of the precursory phenomena in any given seismic region.

Key words *earthquake precursors – earth currents – modelling*

1. Introduction

Seismic risk in a given site is usually defined as the product of hazard by vulnerability. Hazard relates to the seismological and geological features of the site, whereas vulnerability depends on the number and density of resident people and their general conditions, as well as on the value of all goods which can be partly or totally damaged or destroyed by the seismic event. In principle, while the latter parameter can be modified by some external action to obtain a substantial mitigation of the effects deriving from the earthquake, the former parameter can hardly be. Vulnerability, and hence seismic risk, can be lowered by a combined action of earthquake prediction, warning and prevention.

As regards earthquake prediction, Rikitake (1975) quotes the following categories of precursors, according to discipline and observation methods: land deformation, tilt and strain, foreshock, *b*-value, microseismicity, source mechanism, fault creep anomaly, v_p and v_s, v_p/v_s, geomagnetism, earth current, resistivity, radon emission, underground water, oil flow.

It is claimed that the use of these precursors is to a large extent still empirical, owing to the many difficulties that exist in understanding the physics of earthquakes in its entirety. Of course, the lack of a general methodology of observation and interpretation of precursory phenomena on a quantitative basis concurs in explaining why high risk areas do not yet benefit from concrete measures of civil protection.

Among the above categories a prominent role is played by earth current anomalous variations prior to earthquakes. These currents can be revealed on the earth's free surface by

Mailing address: Prof. Domenico Patella, Dipartimento di Geofisica e Vulcanologia, Università di Napoli «Federico II», Largo San Marcellino 10, 80138 Napoli, Italy; e-mail: patella@dgvna.dgv.unina.it

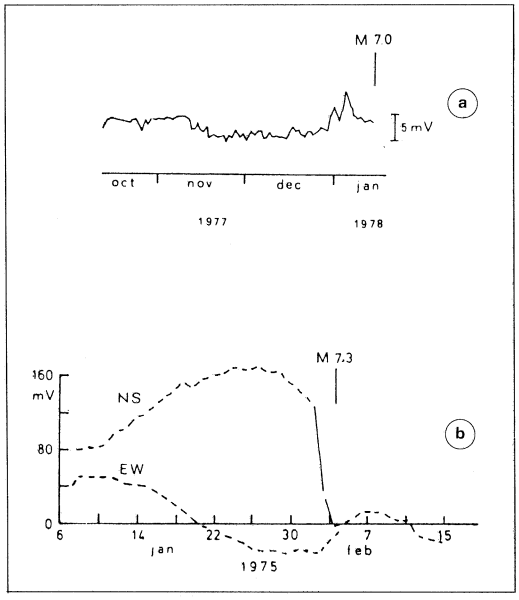

Fig. 1a,b. Examples of field recordings of earth current anomalies preceding earthquakes. a) The anomalous potential difference observed at Nakaizu preceding the Izu-Oshima-Kinkai earthquake (M = 7.0 – 14 January 1978) (after Honkura, 1978). b) The anomalous potential differences between electrode pairs in the NS and EW directions observed at a distance of 25 km from the epicenter of the Haicheng earthquake (M = 7.3 – 4 February 1975) (after Raleigh *et al.*, 1977).

means of voltage measurements at the ends of a passive line, where impolarizable electrodes are grounded. Figure 1a,b shows examples of anomalous earth current recordings prior to some earthquakes.

The circumstances that a strong earthquake in China has been forecasted mainly thanks to earth current measurements (Noritomi, 1978) and that an empirical method of analysis of earth current anomalies (VAN method) is currently applied in Greece to predict local ground motions (Varotsos and Alexopoulos, 1984a,b) are of great interest for the scientific community. Nevertheless, the problem is still far from being solved satisfactorily.

With the aim of approaching a deterministic solution to the problem as close as possible, this note proposes a physical model, capable of explaining the formation of anomalous earth current fields prior to earthquakes. On the basis of this model, we then outline the principles of earth current data acquisition and interpretation method.

2. The Dilatancy-Diffusion-Polarization (DDP) model

The increasing accumulation of strains in a seismic focal region can cause dilatancy of rocks (Nur, 1972). The phenomenon of dilatancy consists in the formation and propagation of cracks inside a rock as stresses reach about half its strength (Brace *et al.*, 1966).

If the rocks in the focal region and surrounding volumes are saturated with fluids, the opening of spaces by dilatancy generates pressure gradients, which the fluid particles are subject to (Lomnitz and Rosenblueth, 1976). Hence, fluids invade the newly opened voids and the flow lasts until the pressure balances inside the whole system of interconnected pores. During fluid invasion the condition of rock dilatancy-hardening can be reached, which prevents the rock from further dilatancy as stress accumulation continues and pore pressure rises inside the cracks (Frank, 1965). The dilated rock strength limit can be thus overcome: the rock suddenly weakens and the earthquake is triggered.

The presence of dissolved salts in the underground liquids makes them rich in anions and cations. The free liquid in the centre of the rock pore is usually enriched in cations, while anions are usually adsorbed on the solid surface in silicate rocks. The free pore water carries an excess positive charge, part of which accumulates close to the solid-liquid interface forming a stable double layer. When the liquids are forced through the porous medium owing to the action of the pressure gradients due to dilatancy, the water molecules carry along with them free positive ions in the diffusion part of the pore. This relative movement of cations with respect to the firmly attached anions generates the well known streaming potential (Keller and Frischknecht, 1966). Of course, the role of the electrical charges can be

reversed, according to the adsorption properties of the rocks.

As suggested by Mizutani *et al.* (1976), the formation of the double layer and the streaming potential accompanying the fluid motion towards the dilatant zone can be responsible for the voltages which are measured on the ground surface preceding an earthquake. Other possible causative factors are temperature gradients especially in volcanic areas, and concentration gradients related to tortuosity and narrowings of the cracks capillary system (Di Maio and Patella, 1991).

In actual field conditions the crack system may very likely present a randomly branched geometry, due to inhomogeneity of the point mechanical properties of the medium as well as to time and space variations of the vector stress field. Moreover, the crack propagation process may be discontinuous in time and may occur at a rate sometimes slower, sometimes faster than the fluid flow in the dilatant region (Lomnitz and Rosenblueth, 1976). These properties might reasonably explain the always scattered behaviour of the observed recordings of earth current anomalies, like those displayed in fig. 1a,b.

Figure 2 depicts our point of view in a qualitative and synthetic way. Four successive stages of the aforesaid dilatancy-fluid diffusion-electrical polarization (DDP) model are shown.

Stage A corresponds to incipient dilatancy. Cracks are being created inside a focal region close, *e.g.*, to a fault plane. They are not yet linked with the water saturated porous system, where separated negative and positive ionic clouds overlap to form a large scale neutral

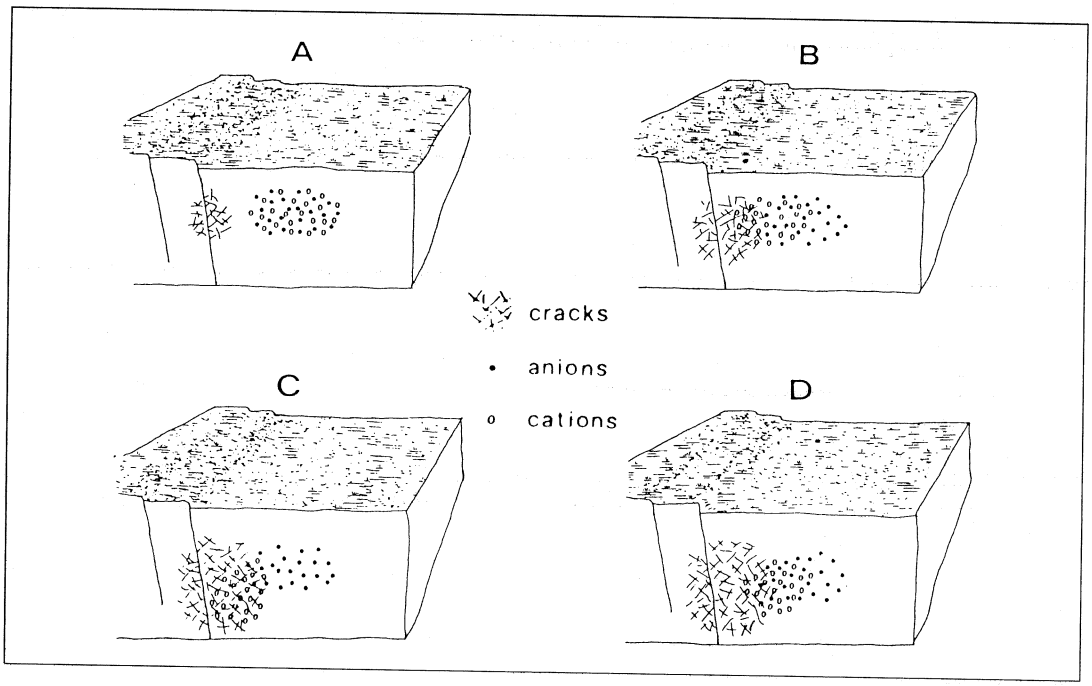

Fig. 2. The dilatancy-fluid diffusion-electric polarization hypothesis for the explanation of the earth current anomaly generation. Four successive stages are depicted: A = incipient crack formation; B = start of fluid diffusion and electrical polarization; C = culmination of fluid diffusion and electrical polarization; D = electrical depolarization phase.

electric compound. No earth current anomaly can be observed on the ground surface.

Stage B corresponds to a growing dilatant volume: new spaces are being opened in such a way that they begin to be connected to the fluid reservoir. Fluid diffusion starts and the net effect of separation of two ionic clouds of opposite sign follows. The previous neutral equilibrium is shattered and an anomalous electric field is generated, that lets earth currents circulate everywhere in the surrounding space. In distant regions the electric current field can be imagined as fed by a bipolar system, with the source and sink points located in the electrical barycentres of the positive and negative ionic clouds, respectively.

Stage C refers to the mature situation, in which both dilatancy and fluid diffusion have reached culmination. The important aspect is that the diffusing ionic cloud occupies a new position with respect to the adsorbed ionic cloud. Both the bipole moment and orientation are changed with respect to the previous stage. A great variety of different bipolar orientations having increasing moments as time elapses can be imagined between stages B and C.

Finally, stage D corresponds to the depolarization process, during which the mobile ionic cloud relaxes as pore pressure gradients drop, in order to re-establish the neutral electrical configuration. The depletion of the anomalous bipolar moment may take place within the entire period of time which separates the rock hardening phase from the earthquake.

On the basis of this conceptual model, which explains the generation of earth current anomalies during the preparation time of an earthquake, in the following section we will give a mathematical development of the phenomenon, by considering the regions of unbalanced charge accumulation as a couple of buried current source and sink.

In the above discussion a time dependent polarization mechanism has been hypothesized. However, experimental observations show that the DDP process is in general sufficiently slow so that a sequence of stationary solutions, each one obtained by assuming constant strength and position of the source and sink, may well represent the whole phenomenon.

3. Mathematical basis of the DDP model in the case of an *n*-layered earth

3.1. *General theory*

The mathematical formulation of the electrical potential due to a buried source is well known among exploration geophysicists. The theory has useful applications in mining geophysics to interpret self-potential anomalies caused by electronically conducting mineral ores (Merkel, 1971). However, for the benefit of readers who are not familiar with the geoelectrical methods, we give here a comprehensive treatment of the theory, opportunely modified in order to match the problem under study.

With reference to fig. 3, let us consider a point electrical source A with strength $\overline{Q}_j$ buried inside the j-th layer ($j = 1, 2, ..., n$) of an n-layered earth at a depth δ from the ground level. The generic i-th layer ($i = 1, 2, .., j, .., n$) is characterized by its conductivity σ_i and depth h_i of its bottom discontinuity ($h_n = \infty$).

We take a cylindrical coordinate system (r, ϑ, z) centered in A_0, the vertical projection of A on the earth's free surface. The position of the observation point M in the underground is defined by the horizontal radial distance r from the vertical axis z, assumed positive downwards, the depth z from the ground surface and the azimuth ϑ, positive clockwise, between the radial distance r and a reference horizontal axis.

Due to horizontal circular symmetry of the field created by the source A, the potential U_i in the i-th layer will not depend on the azimuth ϑ. Moreover, the potential U_i can be thought of as the sum of a normal potential V_0, due to the source A of strength $\overline{Q}_j$ located a distance δ from the origin inside a hypothetically homogeneous space with conductivity σ_j, and a perturbation potential U'_i, due to the presence of the discontinuity planes, *i.e.*

$$U_i = V_0 + U'_i. \tag{3.1}$$

The normal potential in point M is given by

$$V_0 = \frac{\overline{Q}_j}{\sqrt{[r^2 + (z - \delta)^2]}}, \tag{3.2}$$

and the perturbation potential has to satisfy

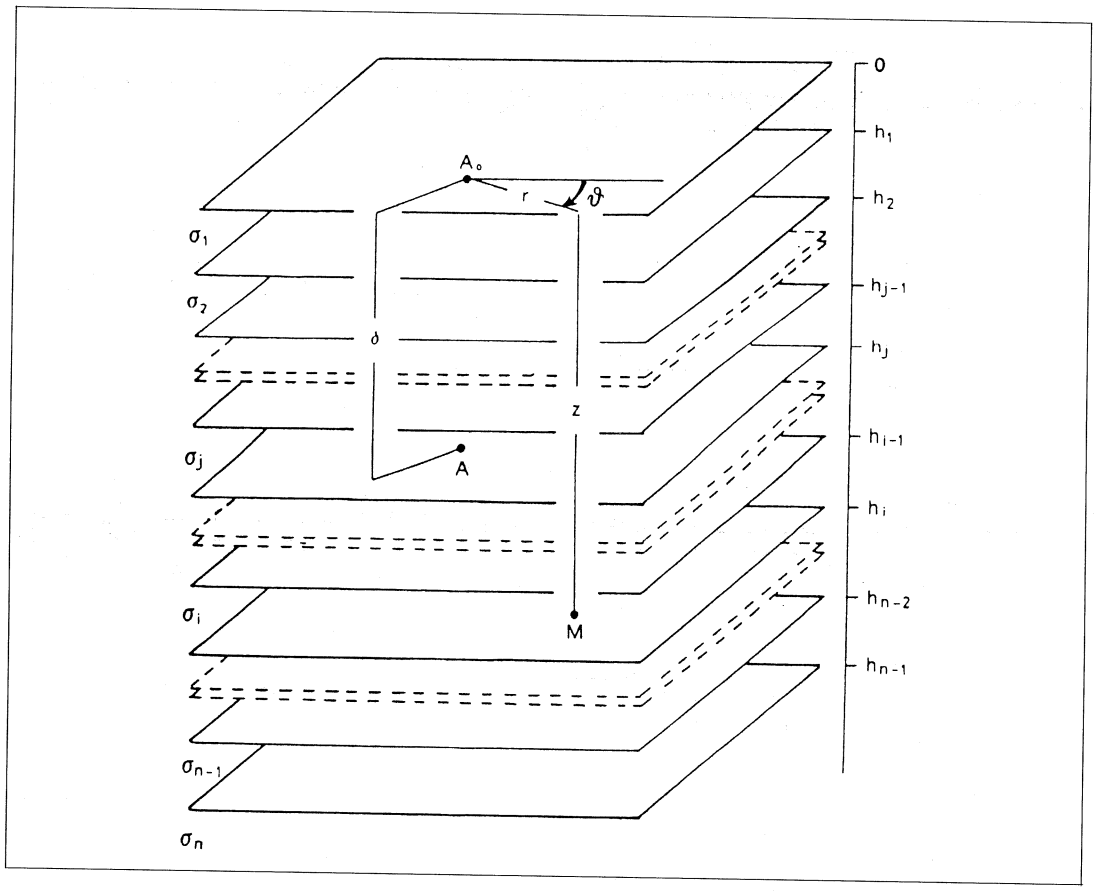

Fig. 3. The n-layered earth model with the monopole source A of electric potential buried inside the generic j-th layer at the depth δ from the ground surface. The reference cylindrical coordinate system (r, ϑ, z) for the solution to the theoretical problem is centered on the surface projection A_0 of the source A. The point M refers to any observation station of the earth current potential.

Laplace's equation, which in cylindrical coordinates is written as

$$\frac{\partial^2 U_i'}{\partial r^2} + \frac{1}{r}\frac{\partial U_i'}{\partial r} + \frac{\partial^2 U_i'}{\partial z^2} = 0. \qquad (3.3)$$

The solution of eq. (3.3) is

$$U_i' = \int_0^\infty [A_i'(m)\exp(-mz) + B_i'(m)\exp(mz)]\, J_0(mr)\, dm, \qquad (3.4)$$

where m is a dummy variable of integration, $J_0(mr)$ is the Bessel function of the first kind and zero order and $A_i'(m)$ and $B_i'(m)$ are unknown coefficients to be determined by the boundary conditions.

Putting

$$A_i'(m) = \overline{Q}_j A_i(m), \qquad (3.5a)$$

$$B_i'(m) = \overline{Q}_j B_i(m), \qquad (3.5b)$$

and combining eqs. (3.2) and (3.4), the poten-

tial U_i is given by

$$U_i = \overline{Q}_j \left\{ \frac{1}{\sqrt{[r^2+(z-\delta)^2]}} + \right.$$

$$+ \int_0^\infty [A_i(m) \exp(-mz) +$$

$$\left. + B_i(m) \exp(mz)] J_0(mr)\, dm \right\}. \quad (3.6)$$

Since it is (Abramowitz and Stegun, 1965)

$$\frac{1}{\sqrt{[r^2+(z-\delta)^2]}} =$$

$$= \int_0^\infty \exp[-m(z-\delta)] J_0(mr)\, dm,$$

$$(z \geq \delta,\ r \geq 0), \quad (3.7)$$

$$= \int_0^\infty \exp[-m(\delta-z)] J_0(mr)\, dm,$$

$$(z \leq \delta,\ r \geq 0), \quad (3.8)$$

with $[r^2+(z-\delta)^2] \neq 0$ in both cases, we can write eq. (3.6) as it follows

$$U_i = \overline{Q}_j \int_0^\infty \{\exp[-m(z-\delta)] + A_i(m) \exp(-mz) +$$

$$+ B_i(m) \exp(mz)\} J_0(mr)\, dm, \quad (3.9)$$

when all observation points lie below or at the same level as the source at most, and

$$U_i = \overline{Q}_j \int_0^\infty \{\exp[-m(\delta-z)] + A_i(m) \exp(-mz) +$$

$$+ B_i(m) \exp(mz)\} J_0(mr)\, dm, \quad (3.10)$$

when all observation points lie above or at the same level as the source at most.

The boundary conditions to be satisfied are:
a) the normal component of the earth currents must vanish at the air-earth discontinuity, *i.e.*

$$\left. \frac{\partial U_1}{\partial z} \right|_{z=0} = 0; \quad (3.11)$$

b) the potential must tend to zero for increasing distances from the source. As this condition is regularly satisfied in every i-th layer ($i = 1, 2, ..., n-1$) for r going to infinity, whatever the values of $A_i(m)$ and $B_i(m)$, we have only to verify that

$$\lim_{\substack{r\to\infty \\ z\to\infty}} U_n = 0; \quad (3.12)$$

c) the potential must be continuous across any interface, *i.e.*

$$U_i|_{z=h_i} = U_{i+1}|_{z=h_i}$$

$$\text{for } i = 1, 2, ..., n-1; \quad (3.13)$$

d) the normal component of the earth currents must be continuous across any discontinuity plane, *i.e.*

$$\sigma_i \left. \frac{\partial U_i}{\partial z} \right|_{z=h_i} = \sigma_{i+1} \left. \frac{\partial U_{i+1}}{\partial z} \right|_{z=h_i}$$

$$\text{for } i = 1, 2, ..., n-1. \quad (3.14)$$

In conclusion we have $2n$ independent boundary conditions and $2n$ unknown coefficients $A_i(m)$ and $B_i(m)$ ($i = 1, 2, ..., n$), which can be thus univocally determined.

Taking the first derivative of eq. (3.10) with respect to z, application of condition (3.11) gives

$$B_1(m) = A_1(m) - \exp(-m\delta). \quad (3.15)$$

With this result we can write the compact expression of the potential $U_1(r, \delta)$ on the ground surface as

$$U_1(r, \delta) = 2\overline{Q}_j \int_0^\infty A_1(m) J_0(mr)\, dm, \quad (r \geq 0). \quad (3.16)$$

Hence, for the calculation of the surface potential due to circulation of earth currents in the subsoil, it is sufficient to determine the coefficient $A_1(m)$.

Applying the boundary condition (3.12), we readily obtain

$$B_n(m) \equiv 0. \tag{3.17}$$

Application of the boundary condition (3.13) readily leads to the following relationship

$$A_i(m)\exp(-mh_i) + B_i(m)\exp(mh_i) = \\ = A_{i+1}(m)\exp(-mh_i) + B_{i+1}(m)\exp(mh_i), \tag{3.18}$$

for $i = 1, 2, ..., n-1$.

Finally, after taking the first derivative of eqs. (3.9) and (3.10) with respect to z, condition (3.14) leads to the following equations:

$$\sigma_i\{\exp[-m(\delta - h_i)] - A_i(m)\exp(-mh_i) + \\ + B_i(m)\exp(mh_i)\} = \\ = \sigma_{i+1}\{\exp[-m(\delta - h_i)] - A_{i+1}(m)\exp(-mh_i) + \\ + B_{i+1}(m)\exp(mh_i)\}, \tag{3.19}$$

for $i = 1, 2, ..., j-1$, and

$$\sigma_i\{\exp[-m(h_i - \delta)] + A_i(m)\exp(-mh_i) + \\ - B_i(m)\exp(mh_i)\} = \\ = \sigma_{i+1}\{\exp[-m(h_i - \delta)] + A_{i+1}(m)\exp(-mh_i) + \\ - B_{i+1}(m)\exp(mh_i)\}, \tag{3.20}$$

for $i = j, j+1, ..., n-1$.

3.2. *The three-layer earth section*

We consider in this section the case of a three-layer earth section, to which we shall make reference in all subsequent developments.

In the first instance we put the source in the overburden at the depth $0 < \delta < h_1 < h_2$. Hence, the source strength is $\overline{Q}_1$. Resorting back to the equalities (3.15), (3.17), (3.18) and (3.20), due to boundary conditions, we obtain the following system:

$$B_1 = A_1 - \exp(-m\delta) \tag{3.21a}$$

$$A_1\exp(-mh_1) + B_1\exp(mh_1) = \\ = A_2\exp(-mh_1) + B_2\exp(mh_1) \tag{3.21b}$$

$$\sigma_1\{\exp[-m(h_1 - \delta)] + A_1\exp(-mh_1) - B_1\exp(mh_1)\} = \\ = \sigma_2\{\exp[-m(h_1 - \delta)] + A_2\exp(-mh_1) - B_2\exp(mh_1)\} \tag{3.21c}$$

$$A_2\exp(-mh_2) + B_2\exp(mh_2) = A_3\exp(-mh_2) \tag{3.21d}$$

$$\sigma_2\{\exp[-m(h_2 - \delta)] + A_2\exp(-mh_2) - B_2\exp(mh_2)\} = \\ = \sigma_3\{\exp[-m(h_2 - \delta)] + A_3\exp(-mh_2)\}. \tag{3.21e}$$

The solution for the coefficient $A_1(m)$ is given by

$$A_1(m) = \exp(-m\delta)\cdot \\ \cdot \frac{1 + K_1K_2\exp[-2m(h_2 - h_1)]}{1 + K_1K_2\exp[-2m(h_2 - h_1)]} \cdots \\ \cdots \frac{+K_1\exp[-2m(h_1 - \delta)] + K_2\exp[-2m(h_2 - \delta)]}{-K_1\exp(-2mh_1) + K_2\exp(-2mh_2)}, \tag{3.22}$$

where

$$K_1 = (\sigma_1 - \sigma_2)/(\sigma_1 + \sigma_2) \tag{3.23a}$$

and

$$K_2 = (\sigma_2 - \sigma_3)/(\sigma_2 + \sigma_3) \tag{3.23b}$$

are the so called reflection coefficients of the boundary planes.

If the source is located inside the second layer ($j = 2$), at a depth $0 < h_1 < \delta < h_2$, the

system of the coefficients becomes

$$B_1 = A_1 - \exp(-m\delta) \tag{3.24a}$$

$$A_1 \exp(-m h_1) + B_1 \exp(m h_1) = \\ = A_2 \exp(-m h_1) + B_2 \exp(m h_1) \tag{3.24b}$$

$$\sigma_1 \{A_1 \exp(-m h_1) - B_1 \exp(m h_1) - \exp[-m(\delta - h_1)]\} = \\ = \sigma_2 \{A_2 \exp(-m h_1) - B_2 \exp(m h_1) - \exp[-m(\delta - h_1)]\} \tag{3.24c}$$

$$A_2 \exp(-m h_2) + B_2 \exp(m h_2) = A_3 \exp(-m h_2) \tag{3.24d}$$

$$\sigma_2 \{\exp[-m(h_2 - \delta)] + A_2 \exp(-m h_2) - B_2 \exp(m h_2)\} = \\ = \sigma_3 \{\exp[-m(h_2 - \delta)] + A_3 \exp(-m h_2)\}. \tag{3.24e}$$

The solution for the coefficient $A_1(m)$ is now given by

$$A_1(m) = (1 - K_1) \exp(-m\delta) \cdot \\ \cdot \frac{1 + K_2 \exp[-2m(h_2 - \delta)]}{1 + K_1 K_2 \exp[-2m(h_2 - h_1)] - K_1 \exp(-2mh_1) - K_2 \exp(-2mh_2)}. \tag{3.25}$$

Finally, if the source is located inside the basement ($j = 3$), at a depth $0 < h_1 < h_2 < \delta$, the system of the coefficients becomes

$$B_1 = A_1 - \exp(-m\delta) \tag{3.26a}$$

$$A_1 \exp(-mh_1) + B_1 \exp(mh_1) = \\ = A_2 \exp(-mh_1) + B_2 \exp(mh_1) \tag{3.26b}$$

$$\sigma_1 \{A_1 \exp(-m h_1) - B_1 \exp(m h_1) - \exp[-m(\delta - h_1)]\} = \\ = \sigma_2 \{A_2 \exp(-m h_1) - B_2 \exp(mh_1) - \exp[-m(\delta - h_1)]\} \tag{3.26c}$$

$$A_2 \exp(-m h_2) + B_2 \exp(m h_2) = A_3 \exp(-m h_2) \tag{3.26d}$$

$$\sigma_2 \{A_2 \exp(-m h_2) - B_2 \exp(m h_2) - \exp[-m(\delta - h_2)]\} = \\ = \sigma_3 \{A_3 \exp(-m h_2) - \exp[-m(\delta - h_2)]\}, \tag{3.26e}$$

and hence the solution for the coefficient $A_1(m)$ is given by

$$A_1(m) = (1 - K_1)(1 - K_2) \exp(-m\delta) \cdot \\ \cdot \frac{1}{1 + K_1 K_2 \exp[-2m(h_2 - h_1)] - K_1 \exp(-2mh_1) - K_2 \exp(-2mh_2)}. \tag{3.27}$$

The three solutions (3.22), (3.25) and (3.27) when inserted into eq. (3.16) allow us to calculate the electric potential on the ground surface due to a buried source located at any depth inside a three-layer earth section.

In practice, we measure the potential difference between two probes M and N placed on the ground surface a distance s apart of the order of some tens up to a few hundreds of meters.

In general we have to admit that the potential may be due to any number L of sources and sinks, located at different depths in the subsoil. Let q ($q = 1, 2, ..., L$) be the relative running index, so that δ_q and $\overline{Q}_{qj}$ will represent depth and strength, respectively, of each of them ($\overline{Q}_{qj}$ is positive for a source and negative for a sink). With such an assumption the potential difference, which we would detect on the ground surface, say $U(M)$-$U(N)$, is given by

$$U(M) - U(N) = \sum_{q=1}^{L} U_1(r_q, \delta_q) - \sum_{q=1}^{L} U_1(r_q + s, \delta_q) = \\ = 2 \sum_{q=1}^{L} \overline{Q}_{qj} \int_0^{\infty} A_{q1}(m) \{J_0(mr_q) - J_0[m(r_q + s)]\}\, dm. \tag{3.28}$$

Equation (3.28) is the most general expression for evaluating potential differences due to a buried multi-pole system within a layered earth. However, to help modelling earth cur-

rent anomalies which are observed prior to earthquakes, a simple bipolar system, pole A positive and pole B negative spaced a distance R from each other, will suffice to represent the DDP phenomenon, according to the model depicted in fig. 2, as we shall point out hereafter by analysing appropriate synthetic examples.

Figure 4 shows the geometry of the buried bipolar source AB and of the crossed dipoles MN in two observation stations C and D on the ground. Besides the length R the bipole source system is also identified by the depth δ of the barycentre B of the fixed negative ionic cloud, *i.e.* the sink, the azimuthal angle α, which the projection of the segment AB over the horizontal plane forms with respect to a reference x-axis, and the dipping angle β, which the AB-axis forms with respect to the vertical z-axis passing through the sink point B.

4. Properties of the DDP generated electric field over a three-layered earth

4.1. *Spatial and temporal features*

For the purposes of this section and following the specifications drawn in the theoretical development, we will make reference to a three-layered earth section, for which four types of conductivity sequences are possible, namely H, K, A and Q. The parameters for this one-dimensional earth model are reported in table I. The numerical values have been selected without any reference to real situations.

Figure 5 shows the behaviour of the potential difference as the distance r of the midpoint between the potential electrodes M and N from the surface projection of the negative pole of

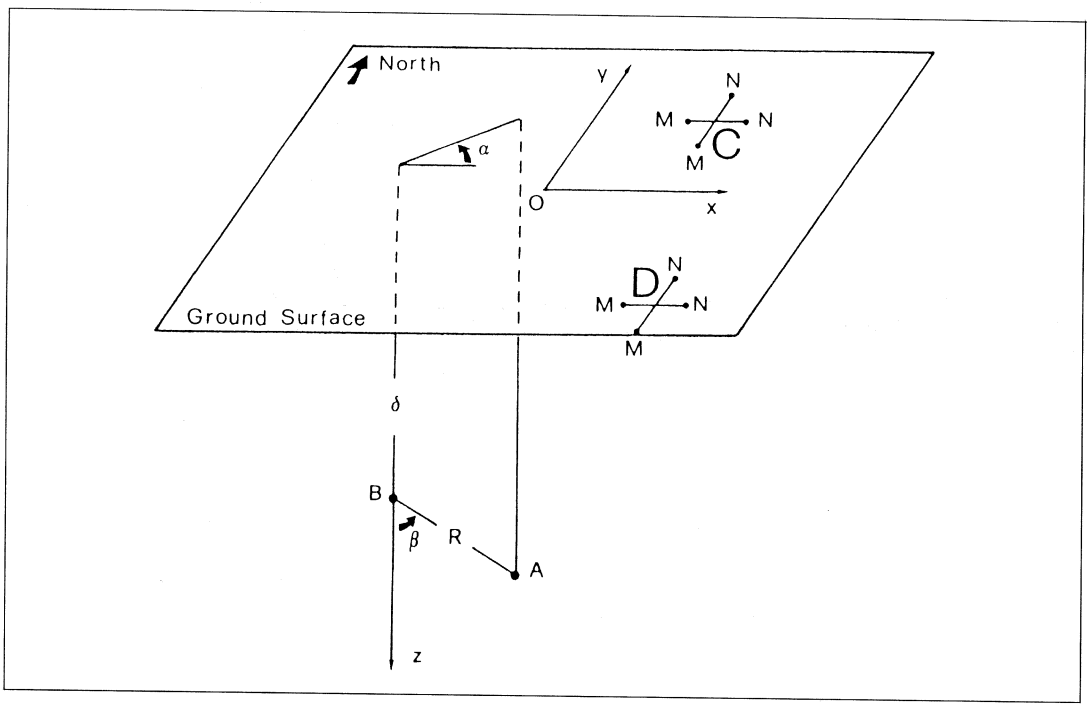

Fig. 4. The geometrical parameters defining the buried bipolar source of anomalous earth current potentials, according to the model of fig. 2. A and B are the electrical barycenters of the mobile and fixed ionic clouds, respectively. The earth current field is observed as potential differences between any two pairs of MN electrodes located on the ground surface in the NS and EW directions, as in the depicted monitoring stations C and D.

Table I. The four types of conductivity distribution of a three-layer earth model and the layering parameters assumed for the computation of the synthetic examples.

Conductivity (mho/m)	Type				Depth of the interfaces (m)
	H	*K*	*A*	*Q*	
1st layer σ_1	10E-3	10E-3	10E-3	10E-3	1000
2nd layer σ_2	10E-2	10E-4	2 · 10E-4	10E-2	5000
3rd layer σ_3	10E-3	10E-3	10E-4	10E-1	∞

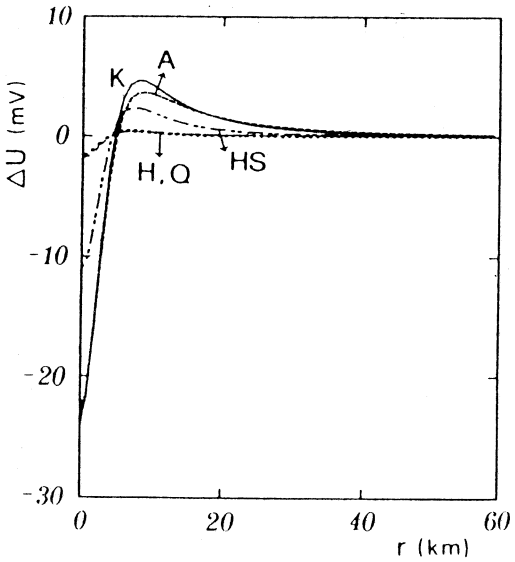

Fig. 5. The behaviour of the potential difference on the ground surface against the distance r of the center of the receiving dipole MN from the surface projection of the negative pole of a bipolar source. Referring to figs. 3 and 4 for the definition of the geometrical parameters, the values assumed here are $\delta = 3$ km, $MN = 200$ m, $R = 1000$ m, $\alpha = 0°$ and $\beta = 90°$. The equivalent current intensity irradiated by the source is $I = 10$ A. I is related to the strength $\bar{Q}$ of a pole source by the relationship $I = 4\pi\bar{Q}\sigma$, σ being the intrinsic conductivity of the rock material where the source is placed. The curves labelled by the letters *H*, *K*, *A* and *Q* refer to the response of a three-layered section, whose layering parameters are reported in table I. The curve labelled by the letter *HS* is the response of the reference homogeneous half-space model.

the bipolar source increases. The potential probes M and N and the surface projection of the bipolar source AB are aligned along the same straight-line. As one readily can see, the highest amplitudes are obtained over *A* and *K* type sections, whereas in *H* and *Q* sections the signal practically vanishes.

The diagram corresponding to the homogeneous half-space with conductivity 10E-3 mho/m, labelled by the abbreviation *HS*, is reported for comparison. With reference to the *HS* diagram, we note that for *A* and *K* sections the localization of the source inside the less conductive intermediate layer provides an enhancement of the signal on the free surface. Conversely, for *H* and *Q* sections the presence of the source inside the less resistant second layer provokes a notable damping of the same signal.

In other words, a DDP process, which develops in a conductive layer underlying a resistant overburden, generates earth currents, which are short-circuited within the same layer and cannot be measured on the ground surface. In case of an earthquake no earth current precursor would be observed in a monitored area of this type.

Of course the sign of the anomaly depends on the orientation of the MN dipole and AB bipole axes (here we always assume *A* positive and *B* negative).

With reference to the two observation stations C and D shown in fig. 4, where two MN alignments are traced in order to schematize the standard rule of making records in the north-south direction as well as in the east-west direction, fig. 6 depicts the behaviour of

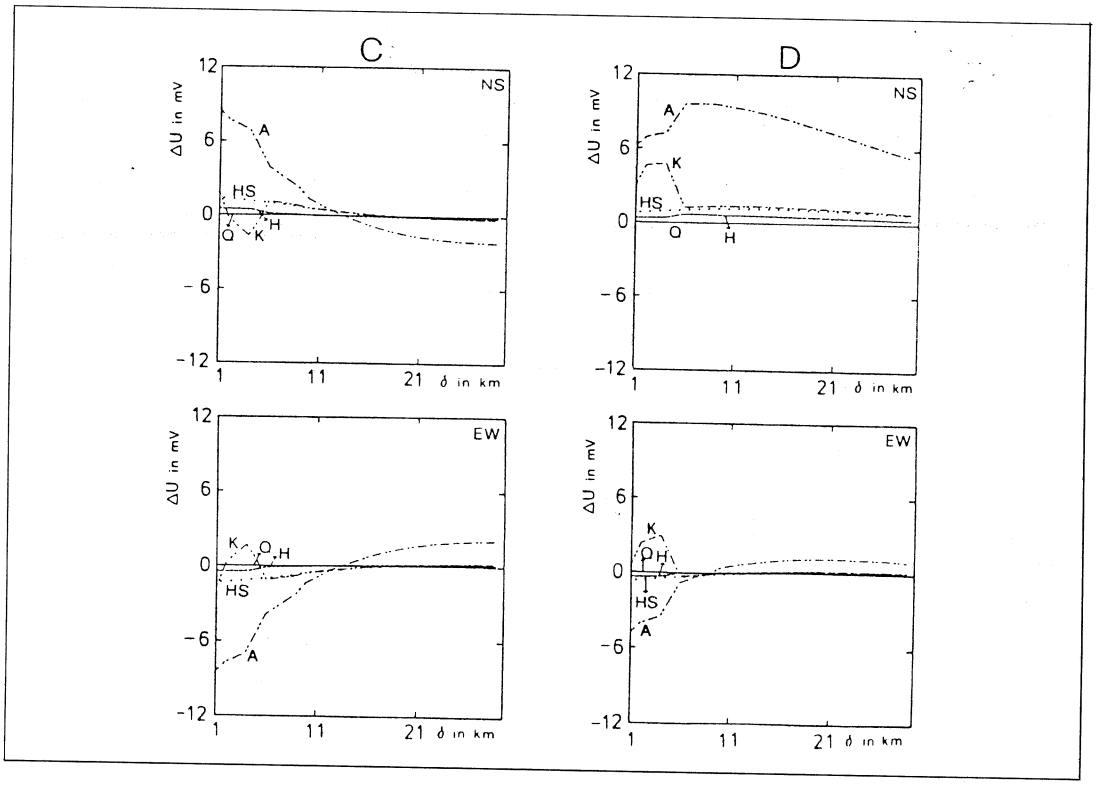

Fig. 6. The behaviour of the potential difference on the ground surface against the depth δ of the fixed negative pole of a buried bipolar source. The left and right-hand pairs of diagrams refer to stations C and D of fig. 4, respectively. In both pairs, the upper diagram refers to the NS alignment of the *MN* receiving dipole, whereas the lower diagram refers to the EW alignment. The plane coordinates of the fixed pole source *B*, with respect to an arbitrarily chosen reference system like the one depicted in fig. 4, are $x = 450$ m and $y = 0$. Making reference again to fig. 4, the values assumed for the other geometrical parameters are $MN = 200$ m, $R = 1000$ m, $\alpha = 45°$ and $\beta = 45°$. The equivalent current intensity emanating from the source is $I = 100$ A. For the definition of *I* refer to fig. 5. Curve identification labels are the same as in fig. 5 as all diagrams refer to the responses of a three-layered earth, whose layering parameters are reported in table I. The plane rectangular coordinates of stations C and D with respect to the same reference system of the pole source *B*, are $x = 25$ km, $y = 25$ km and $x = 40$ km, $y = -40$ km, respectively.

the DDP response on the ground surface as the bipolar source deepens, starting from the first discontinuity level and proceeding downwards in the substratum, after crossing the second discontinuity. In this case, the measuring dipole *MN* and the bipole source *AB* are no longer contained in the same plane in both the observation stations C and D.

A notable difference emerges between the *A*-type response and all the other three-layer type responses, including the response of the reference homogeneous half-space with conductivity 0.0001 mho/m. In fact, in the *A*-type response the signal remains remarkably enhanced over the whole depth range of the bipole source *AB*, adopted for this type of representation. On the contrary, in all of the other three-layered sections the responses always completely vanish, even at the smallest depths, except for the *K*-type section, over which a de-

tectable signal may be recorded as long as the source remains confined within the second layer.

Another important aspect, which deserves some consideration, is the evidence that for *A*-type sections the response can undergo a sign reversal between the two orthogonal measuring directions in a given station, as well as along the same measuring direction between two different station sites. Of course, this depends on the mutual disposition and orientation of the measuring *MN* dipole and the *AB* bipole source.

From this very first analysis we may tentatively approach a preliminary conclusion as follows: for a given source strength and localization inside a three-layered earth, and for given mutual disposition and orientation of the *MN* measuring dipole and *AB* source bipole, the double decreasing conductivity sequence is for earth current detection the most prone underground situation.

This would mean that before starting with any program involving measurements of earth currents as precursors of earthquakes in high seismicity areas, it seems reasonable to undertake a detailed geoelectrical survey of the area, in order to understand the feasibility of the program on the basis of the resulting conductivity sequences. Deep geoelectrical or magnetotelluric soundings are suitable tools for this purpose.

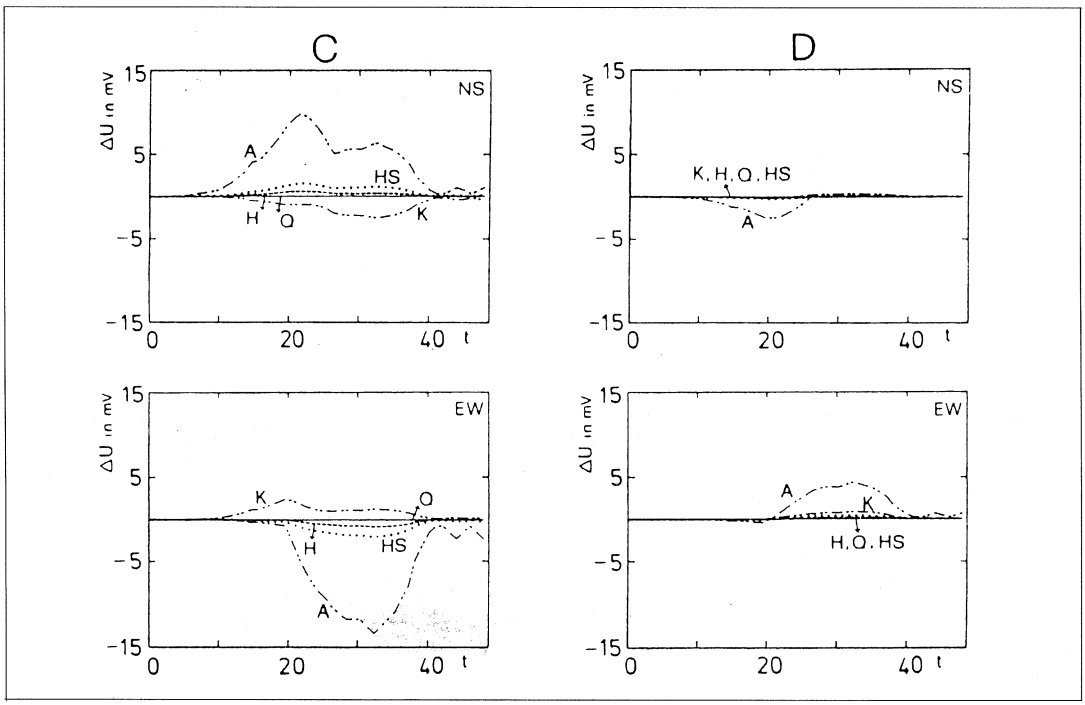

Fig. 7. A simulated time series of potential differences on the ground surface. The left and right-hand pairs of diagrams refer to stations C and D of fig. 4, respectively. The plane coordinates of the stations C and D and those of the fixed pole source B are reported in the caption to fig. 6. For the series of the geometrical parameters, which determine the time evolution of these simulated earth current anomalies, refer to table II and the relative caption. Curve identification labels are the same as in fig. 5 as all diagrams refer to the responses of a three-layered earth, whose layering parameters are reported in table I.

So far we have examined the static situation, which concerns the spatial behaviour of the potential difference on the Earth's surface by admitting a fixed bipolar source as in the stages B or C of fig. 2.

Let us now study the earth current response on the ground surface by taking into consideration the whole DDP time evolution in the seismic focal region. What we are going to show is a simulation of earth current anomalies in such a way as to resemble the real field observations, as those reported in fig. 1a,b.

Figure 7 reports the time evolution of the earth current precursor in the two stations C and D of fig. 4. The time unit along the horizontal axis is arbitrary. The diagrams refer again to the four possible three-layer types. As usual, the reference solution for the half-space is drawn for comparison. A three-stage evolution is proposed. The first stage refers to the developing polarization process, during which only a progressive increase in the moment of the bipole source is assumed for simplicity. The next stage corresponds to the mature situa-

Table II. Time series of the azimuth α, spacing R and equivalent current intensity I of a buried bipolar source of synthetic earth current anomalies having pole B fixed and pole A mobile. The depth δ of the fixed pole B, the dipping angle β of the dipole AB and the amplitude of the monitoring dipoles MN on the ground surface are constantly taken equal to 3000 m, 45° and 200 m, respectively (see fig. 4 for the definition of the bipolar source geometrical parameters). The equivalent current intensity I of a source pole is related to its strength $\overline{Q}$ by the relationship $I = 4\pi\overline{Q}\sigma$, σ being the intrinsic conductivity of the rock material where the source pole is placed. The constant sampling time interval from the starting monitoring instant 1 to the final one N is arbitrary. The source parameters δ, α and I, used for the computation of the six diagrams in each of the figs. 9, 11, 12, 16 and 17, are reported in correspondence with the six time instants t_1, ..., t_6.

t	α (°)	R (m)	I (A)	t	α (°)	R (m)	I (A)
1	0	10	10	$i+1$	60	1500	750
	0	50	30		70	1600	750
	0	70	50		70	1700	750
	0	80	90		70	1800	750
t_1	0	90	150	t_4	70	1800	750
	0	100	200		70	1800	750
	0	120	250		70	1800	800
	0	150	300		70	1800	850
	0	200	300		70	1800	800
	0	250	300		70	1800	750
	0	300	300		70	1800	700
	0	400	350	t_5	70	1800	600
	0	500	400		70	1800	500
	0	600	450		70	1800	300
	0	700	500		70	1800	200
	0	800	600		70	1800	100
	0	900	550		70	1800	50
t_2	0	1000	600		70	1800	50
	0	1100	650		70	1800	100
	0	1200	700		70	1800	150
	0	1300	750		70	1800	100
	10	1400	750		70	1800	50
	20	1500	750		70	1800	100
	30	1500	750	t_6	70	1800	150
t_3	40	1500	750		70	1800	100
i	50	1500	750	N	70	1800	50

tion, during which, in order to simulate the experimentally observed variations, we postulate, at least in this example, at first a continuous modification of the azimuth of the bipole source with practically constant moment and then a small further increase of the moment itself with constant azimuth. The final stage refers to the depolarization process, during which only a notable decrease of the moment of the bipole source is assumed. Table II reports the values given to all the concerned parameters during the three-stage evolution of the DDP process.

To a certain extent, the above simulation may well explain the various anomalies of different form and sign, which are often recorded along the two orthogonal directions in a given site, or in two different stations. Again the *A*-type three-layer sequence gives the best performance, followed by the *K*-type section.

The procedure so far exposed regards the theoretical problem of constructing the synthetic DDP response, given the parameters of the source. However, in practice we have to tackle the inverse problem, *i.e.* the determination of the unknown source parameters by modelling the field records. For this purpose it is necessary to know beforehand the geometry of the conductivity distribution underground by geoelectric and/or magnetotelluric prospects, as previously outlined. Furthermore, a correct localization of the source area is needed, in order to select recording stations in which the useful signal is the highest possible.

4.2. *The field procedure*

There is a criticism about the general validity of earth current observations as precursors of earthquakes. It concerns the occurrence of signals due to other sources, which are not related with the earthquake, *e.g.* raining. Indeed, electrofiltration phenomena can also arise when there is percolation of rain water into

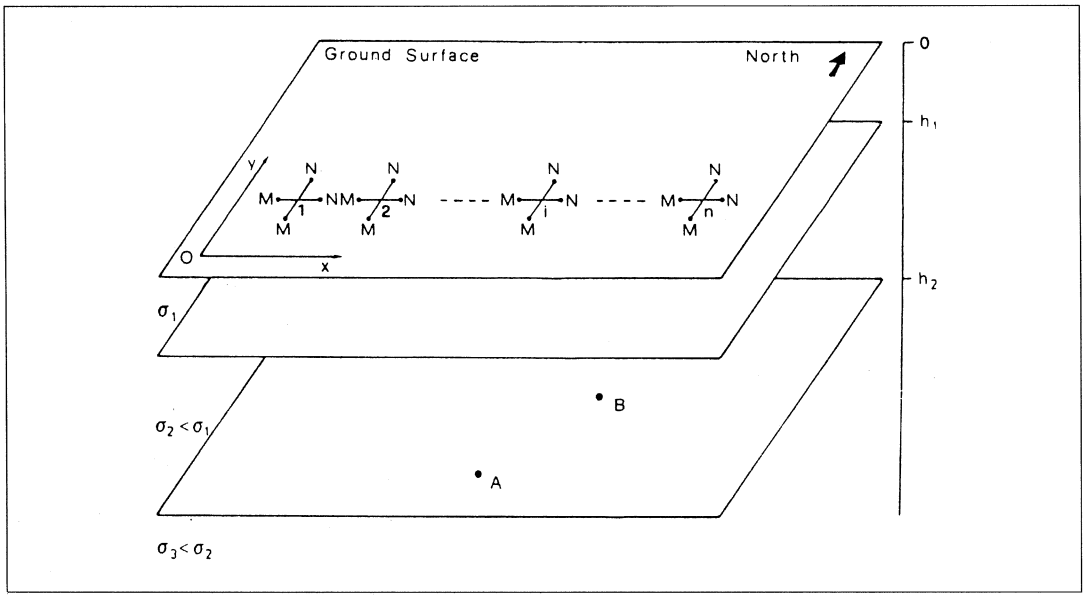

Fig. 8. Description of the profile technique of monitoring the earth current potential differences along the NS and EW alignments of the receiving dipole *MN*. The underground model refers only to an *A*-type three-layer earth as it exhibits the most pronounced surface response.

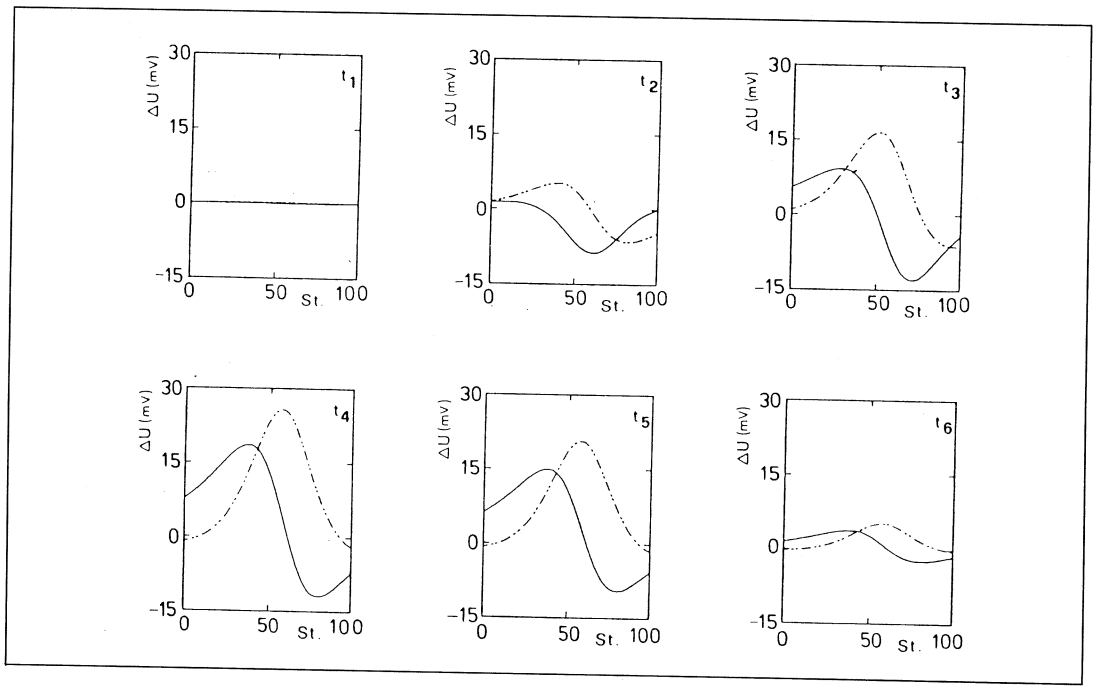

Fig. 9. A synthetic example of the profile scheme of monitoring earth current potential differences along the NS (full lines) and EW (dash-dotted lines) alignments of the receiving dipole *MN*, placed over an *A*-type three-layered earth model, whose layering parameters are reported in table I. Referring to an arbitrary rectangular coordinate system, with the x, y plane over the ground surface and the z-axis positive downward, with respect to which the fixed pole B of the bipolar source has the coordinates $x = 450$ m, $y = 0$ and $z = 3000$ m, the selected profile is a segment of a straight line, the extremes of which have plane coordinates $x = -10$ km, $y = -50$ km and $x = 40$ km, $y = 0$, respectively. The computing sampling interval is 500 m along both the x and y-axis. For the other geometrical parameters of the source-receiver system as well as for the selection of the time instants from t_1 to t_6 refer to table II.

porous rocks; thus earth current anomalies can be measured, which apparently one is not able to distinguish from the anomalies generated by some seismic activity. This is particularly true when records are made in one single station, as is usually the case.

There is no doubt that the nature and geometry of the source differs according to whether it is related to a seismic focal area of relatively limited extent, or to a large region of uniform meteorological activity. Thus, generally speaking the advocated equivalence of the responses may be reasonably explained as due to inadequate monitoring field layouts rather than as due to source equivalence. Concluding, a sequence of stations along a selected profile crossing the focal area, or better a regular network of stations over the focal region can substantiate the occurrence of the electrical precursors much better than a single station.

Figure 8 shows an example of monitoring field layout, according to a profiling technique across the area where a bipolar source, buried inside the sandwiched layer of an *A*-type three-layer earth model, is supposed to be active.

Accordingly, fig. 9 illustrates the time sequence of the synthetic profiling response for a bipole source, to the geometrical parameters

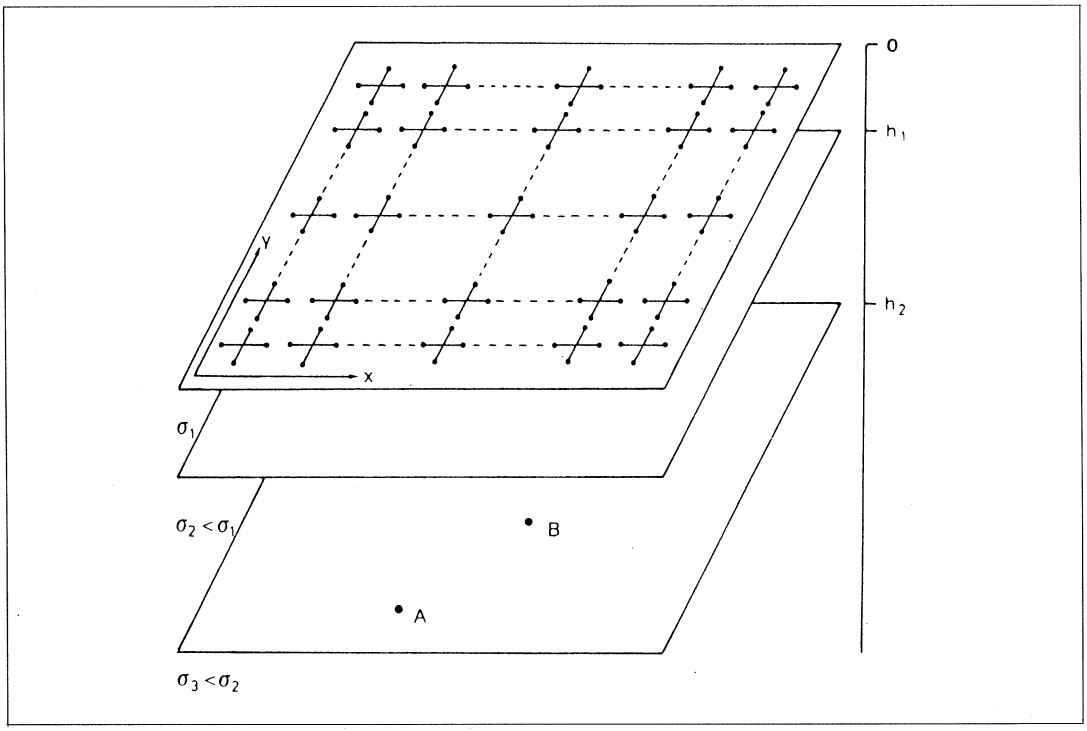

Fig. 10. Description of the mapping technique of monitoring the earth current potential differences along the NS and EW alignments of the receiving dipole *MN*. The underground model refers only to an *A*-type three-layer earth as it exhibits the most pronounced surface response.

and moment of which the same set of values as in table II have been assigned.

Six selected sketches of the complete time evolution of the DDP phenomenon are reported, which correspond to the instants t_1 through t_6 singled out from table II. In each sketch the two lines refer to the north-south (full) and west-east (dashed) measuring directions.

Each picture shows well shaped, large anomalies in correspondence with the source area, which rapidly damp as the distance of the stations from the source area increases.

Although this recording field layout and corresponding anomaly representation can easily let us ascertain the position along the profile where the source is most active, no information can, however, be obtained as to where the source is really located, because of a lack of lateral information from one and the other side of the selected profile.

An areal disposition of the stations such as that in fig. 10 can be assumed as the most suitable monitoring field layout for contouring the source region.

Considering a bipole source plunged once again into an *A*-type three-layer earth structure, figs. 11 and 12 show, respectively, the NS and WE synthetic contour maps of the electrical potential, referred to the sequence of instants t_1 through t_6 of table II. As is readily observed, the focal area is now univocally outlined, in both the orthogonal directions of the measuring dipole. The time evolution of the field is also very well delineated, as concerns both the amplitude and the azimuthal angle variations of the bipole source.

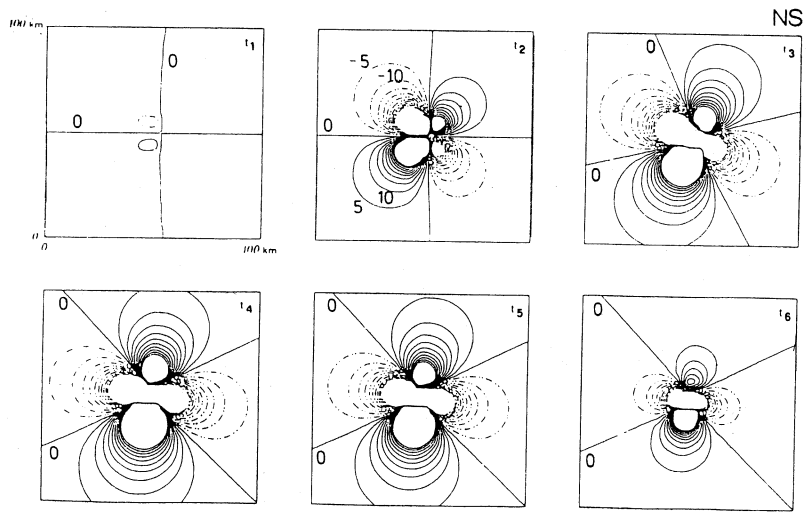

Fig. 11. A synthetic example of the mapping technique of monitoring earth current potential differences. The sequence of maps refers to a NS alignment of the receiver dipole *MN*, placed over an *A*-type three-layer earth, the layering parameters of which are given in table I. Referring to an arbitrary rectangular coordinate system, with the x, y plane over the ground surface and the z-axis positive downward, the fixed pole B of the bipole source has coordinates $x = 450$ m, $y = 0$ and $z = 3000$ m. The mapping area is a square with sides of 100 km parallel to the x and y-axis of the coordinate system, whose origin is placed in the center of the square. A grid of sub-squares of 5 km side has been adopted to compute the potential drops at the receiver dipoles, whose midpoints coincide with the nodes of the mesh. For other parameters of the source system, corresponding to the selected times from t_1 to t_6, refer to table II. Contour interval is 5 mV.

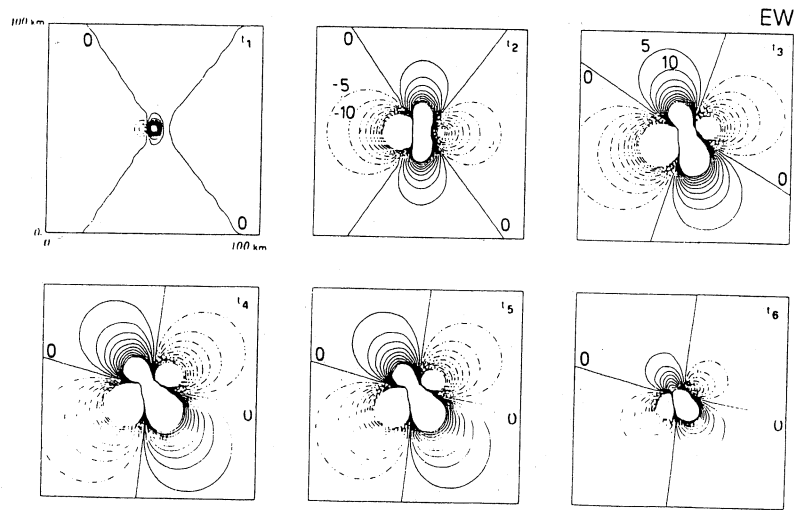

Fig. 12. A synthetic example of the mapping technique of monitoring earth current potential differences. The sequence of maps refers to the EW alignment of the receiving dipole *MN*. Refer to fig. 11 for other relevant parameters.

5. Mathematical basis of the DDP model in the case of a faulted geometry

5.1. *General theory*

The faulted half-space model is represented in fig. 13. A vertical discontinuity plane separates two different regions, each composed of a sequence of n horizontal layers. A conductivity distribution σ_{iu}, where $i = 1, 2, ..., j, ..., n$ specifies the layer and $u = 1, 2$ the region, corresponds to each region. We assume that the j-th layer in region 1 contains the source A of strength $\overline{Q}_{j1}$ at depth δ_1 from the ground surface and horizontal distance d_1 from the fault vertical plane.

Moreover, we admit that the condition (Alfano, 1959)

$$\sigma_{i1}\,\sigma_{(i+1)2} = \sigma_{(i+1)1}\,\sigma_{i2} \qquad (5.1)$$

is satisfied at every intersection line between a horizontal discontinuity and the vertical fault plane. Straight consequences of condition (5.1) are that (Patella and Tramacere, 1986):

1) the reflection coefficient of any horizontal discontinuity is a constant for that plane, *i.e.*,

$$K_{iu} = (\sigma_{iu} - \sigma_{(i+1)u}) / (\sigma_{(i+1)u} + \sigma_{iu}) = \text{const} \qquad (5.2)$$

with $i = 1, 2, ..., j, ..., n-1$ and $u = 1, 2$;

2) the reflection coefficient of the vertical discontinuity plane is also a constant for the plane, *i.e.*,

$$K_{1,2} = (\sigma_{i1} - \sigma_{i2}) / (\sigma_{i1} + \sigma_{i2}) = \text{const} \qquad (5.3)$$

with $i = 1, 2, ..., j, ..., n$.

Under assumption (5.1) it is possible to find the solution to the potential distribution, generated by the buried point source, using the method of images.

Let us suppose first that the observation point M is located in the same region as the source A. The total potential in M is computed as the sum of the potential $U_1(r, \delta_1)$ due to the

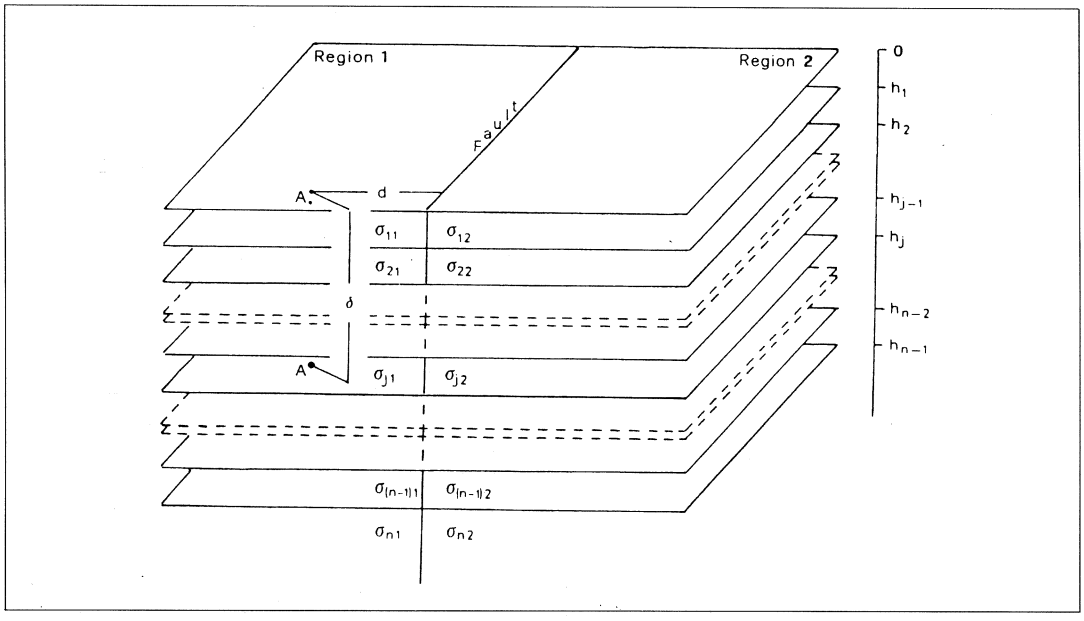

Fig. 13. The faulted earth model. Both regions 1 and 2 from one and the other side of the fault vertical plane are made up of a sequence of n layers.

real source A, given by the following equation, equivalent to (3.16),

$$U_1(r, \delta_1) = 2\overline{Q}_{j1} \int_0^\infty A_1(m) J_0(mr)\, dm, \quad (r \geq 0), \tag{5.4}$$

and the potential $U_1(r', \delta_1)$ due to the image source A' located on the other side of the fault plane symmetrical to A, given by

$$U_1(r', \delta_1) = 2\overline{Q}_{j1} K_{1,2} \int_0^\infty A_1(m) J_0(mr')\, dm, \quad (r' \geq r \geq 0), \tag{5.5}$$

i.e.

$$U_1(r', \delta_1) = 2\overline{Q}_{j1} \int_0^\infty A_1(m) [J_0(mr) + K_{1,2} J_0(mr')]\, dm. \tag{5.6}$$

In eqs. (5.5) and (5.6), r' represents the horizontal distance of the surface projection of the image source A' from the observation point M. It is given by

$$r' = \sqrt{[r^2 + 4d_1 (d_1 - r\cos\phi)]}, \tag{5.7}$$

where ϕ is the angle between the line connecting A and A' and the line connecting A and M.

When the observation point M is located on the other side of the vertical discontinuity plane with respect to the point source A, the total potential in M is a factor $(1+K_{1,2})$ times the potential given by eq. (3.16), that is to say

$$U_1(r, \delta_1) = 2\overline{Q}_{j1} (1 + K_{1,2}) \int_0^\infty A_1(m) J_0(mr)\, dm, \quad (r \geq 0). \tag{5.8}$$

5.2. *The faulted half-space*

In this simplest case, the coefficient $A_1(m)$ appearing into eqs. (5.4), (5.5) and (5.8) by virtue of the boundary conditions (3.11) and (3.12), is given by

$$A_1(m) = \exp(-m\delta_1). \tag{5.9}$$

Hence, taking into account the identity (3.8), we readily obtain

$$U_1(r, \delta_1) = 2\overline{Q}_{11} \left[\frac{1}{\sqrt{(r^2 + \delta_1^2)}} + \frac{K_{1,2}}{\sqrt{r'^2 + \delta_1^2}} \right], \tag{5.10}$$

when the observation point M lies on the free surface of the same region where the source point A is located, and

$$U_1(r, \delta_1) = 2\overline{Q}_{11} \frac{1 + K_{1,2}}{\sqrt{(r^2 + \delta_1^2)}}, \tag{5.11}$$

when M lies on the surface of the opposite region.

The simplest solutions (5.10) and (5.11) can be readily utilized to compute the potential distribution on the ground surface, over one and the other side with respect to the vertical discontinuity plane.

6. Properties of the DDP generated electric field over a faulted half-space

Following the same approach used in the previous sections to specify the temporal and spatial variation of the earth current potentials for the case of the three-layered earth, we give in this section some outlines for the case of the faulted half-space.

Making reference to fig. 14 for the position of the observation stations and for the parameters assigned to the resistivity model, fig. 15 shows the time evolution of the anomalous potential in the pair of stations C and D, situated in the region of the faulted half-space, where the fixed cloud of negative charges is concen-

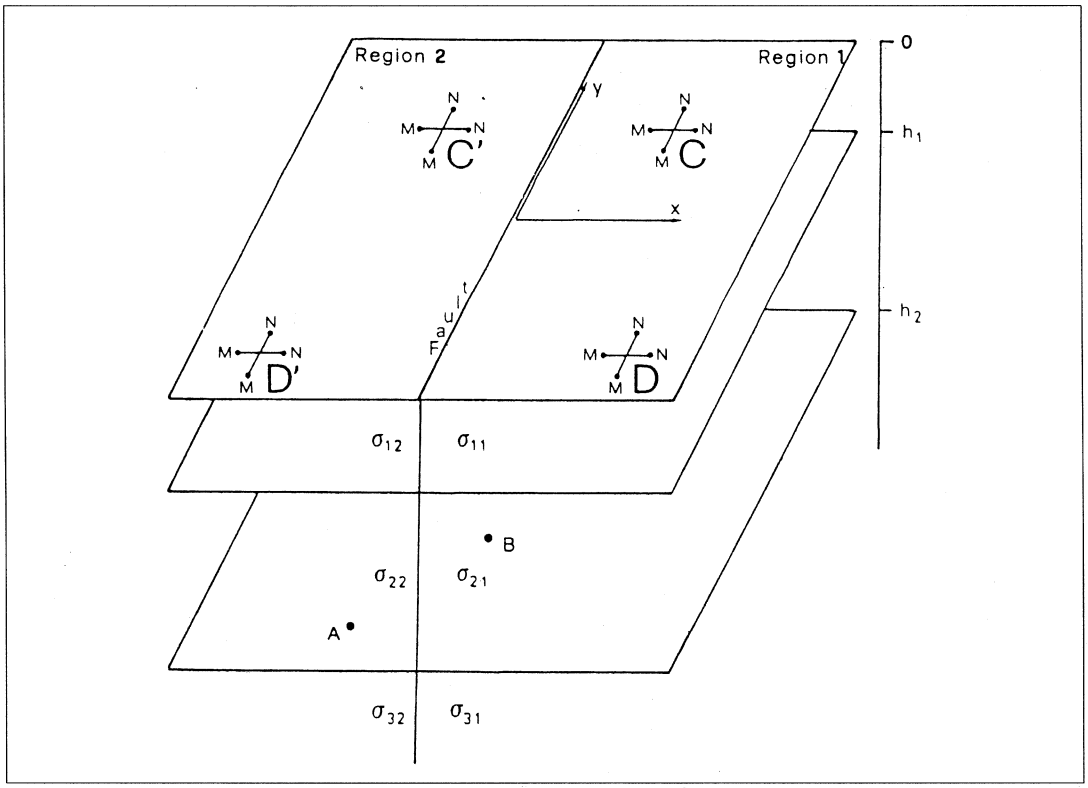

Fig. 14. A simplified fault model. Both regions 1 and 2 are made up of a three-layer sequence of *A*-type. The layering parameters in region 2, on whose free surface stations C′ and D′ are located, are those listed in table I. In region 1, where stations C and D are placed, the thicknesses of the layers are unchanged, while the intrinsic conductivities are all multiplied by a factor of 0.1.

trated, and in the pair of stations C′ and D′, placed on the opposite region, where the positive ionic cloud is diffusing.

Again, the responses along the alignments in the north-south and east-west directions are considered, and the time unit along the horizontal axis is arbitrary. The same three-stage evolution of the previous simulation is taken. The only difference is that now the positive ionic cloud enters progressively into the second region across the fault, as time elapses during the stage of increasing moment. The reverse happens during the relaxation stage. Table II reports the values taken by the source parameters during the three-stage DDP process.

Indeed, this new simulation is practically indistinguishable from those depicted in fig. 7 in the sense that no particular distortion discloses the presence of the fault. Also this effect can be explained as due to the scarce information related to the usual single station recording approach.

However, if one faces the problem by the mapping approach it would be then possible to recognize the presence of the fault. In fact, as shown in the time set of maps of figs. 16 and 17, narrow strips, where the contour lines are strongly distorted, mark well enough the strike of the fault, which can be thus correctly positioned.

7. Conclusions

In the previous sections we have presented the basic theory for a detailed interpretation of earth current anomalies in earthquake prediction studies. We have also suggested a possible field technique for a complete assessment of the information carried by the recordings. The mapping approach seems to be an adequate tool for contouring the focal area, under the assumption that a nucleus of polarized charges is activated in a limited volume of the subsoil in conjunction with growing dilatancy in locally stressed rocks.

There is no doubt that the monitoring of earth current anomalies may provide a useful contribution to earthquake prediction, notwithstanding it is still one of the most controversial topics in applied seismology, especially since the appearance of the VAN technique (Varotsos and Alexopoulos, 1984a,b).

We think that the not yet complete recogni-

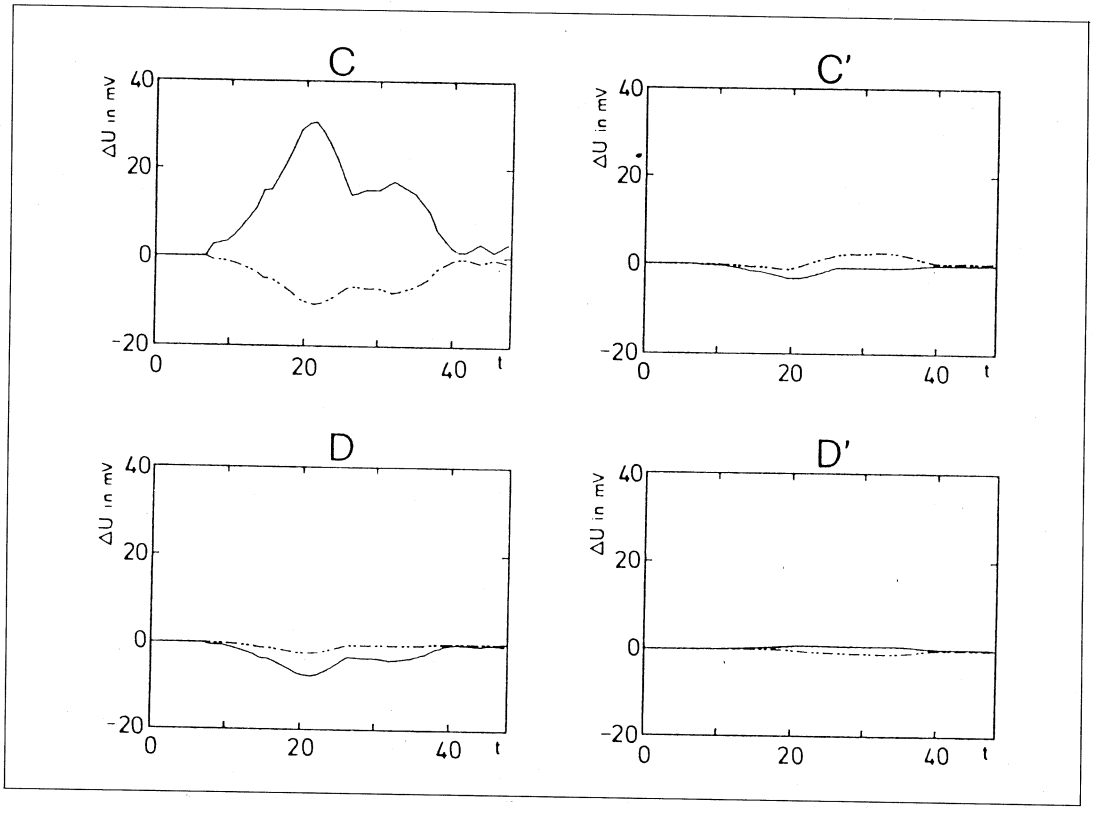

Fig. 15. A simulated time series of earth current potential differences on the ground surface. The left-hand pair of diagrams refers to stations C and D in region 1 of the model in fig. 14, while the right-hand pair refers to stations C′ and D′ in region 2. The full line refers to the NS alignment of the receiving *MN* dipole, while the dashed line to the EW alignment. The coordinates of the fixed sink *B* of the bipolar source, with respect to the reference system traced in fig. 14, in which the *y*-axis coincides with the strike line of the fault, the *x*-axis is positive in region 1 and the vertical *z*-axis is positive downward, are $x = 450$ m, $y = 0$ and $z = 3$ km. The plane coordinates of station C are $x = 25$ km and $y = 25$ km, of D $x = 40$ km and $y = -40$ km, of C′ $x = -25$ km and $y = 25$ km and of D′ $x = -40$ km and $y = -40$ km. For the series of the geometrical parameters, which determine the time evolution of this simulated earth current anomaly, refer to table II.

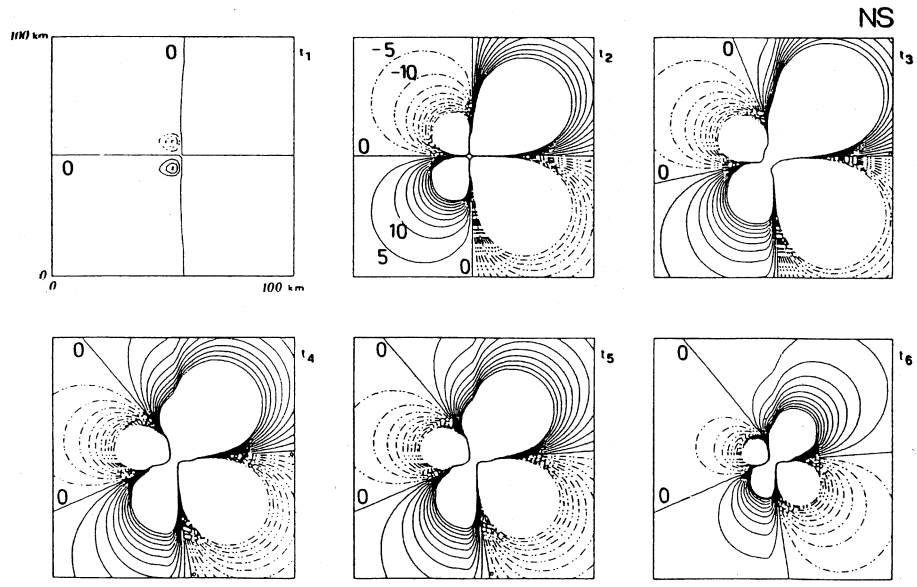

Fig. 16. A synthetic example of the mapping technique of monitoring earth current potential differences. The sequence of maps refers to the NS alignment of the receiving dipole *MN*, placed over a faulted *A*-type three-layer earth model, whose layering parameters are listed in fig. 14. For the criteria used to draw the sequence of the maps, refer to fig. 11. For other parameters of the source, in correspondence with the selected time instants from t_1 to t_6, refer to table II. Contour interval is 5 mV.

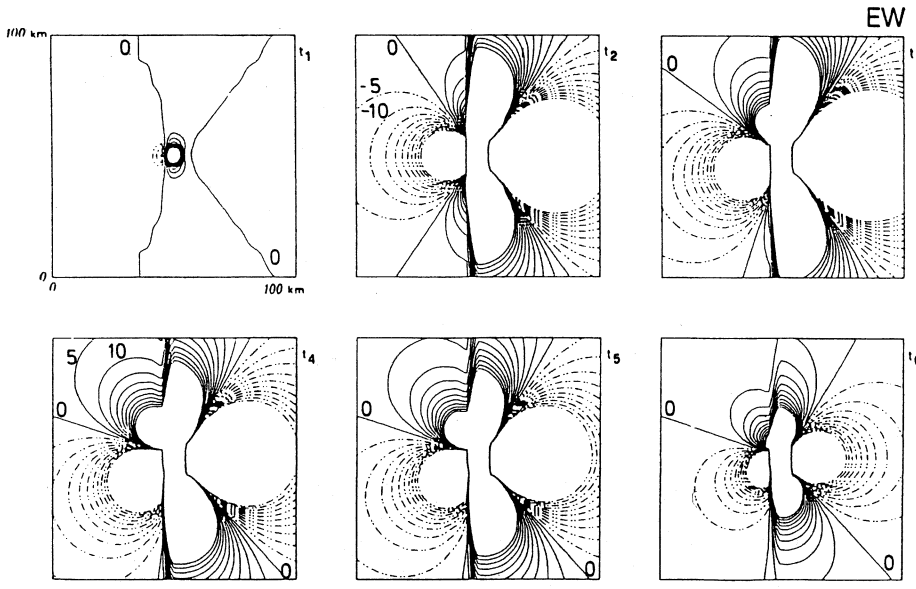

Fig. 17. A synthetic example of the mapping technique of monitoring earth current potential differences. The sequence of maps refers to the EW alignment of the receiving dipole MN, placed over a faulted *A*-type three-layer earth model. Refer to figs. 11 and 16 for the relevant parameters.

tion of the method in earthquake prognostics is mostly due to the lack of a theoretical basic scheme, in which the role of the electric and geometrical properties of the geological structures concerned is properly outlined.

The main purpose of the present paper was to provide a frame within which to set the procedure of data interpretation on a geophysical and geostructural basis. We hope that the proposed procedure may contribute to fill the gap, which still exists from the occurrence of a precursory activity to its interpretation as a definite premonitory effect.

REFERENCES

ABRAMOWITZ, M. and I. STEGUN (1965): *Handbook of Mathematical Functions* (Dover Publ. Inc., New York).

ALFANO, L. (1959): Introduction to the interpretation of resistivity measurements for complicated structural conditions, *Geophys. Prospect.*, **7**, 311-366.

BRACE, W.F., B.W. PAULDING JR. and C.H. SCHOLZ (1966): Dilatancy in the fracture of cristalline rocks, *J. Geophys. Res.*, **71**, 3939-3953.

DI MAIO, R. and D. PATELLA (1991): Basic theory of electrokinetic effects associated with earthquakes, *Boll. Geofis. Teor. Appl.*, **33**, 145-154.

FRANK, F.C. (1965): On dilatancy in relation to seismic sources, *Rev. Geophys.*, **3**, 484-503.

HONKURA, Y. (1978): On a relation between anomalies in the geomagnetic and telluric field observed at Nakaizu and the Izu-Oshima-Kinkai earthquake of 1978, *Bull. Earthq. Res. Inst. Univ. Tokyo*, **53**, 931-937.

KELLER, G.V. and F.C. FRISCHKNECHT (1966): *Electrical Methods in Geophysical Prospecting* (Pergamon Press, Oxford), pp. 523.

LOMNITZ, C. and E. ROSENBLUETH (Editors) (1976): *Seismic Risk and Engineering Decisions* (Elsevier Sc. Publishing Company, Amsterdam), pp. 425.

MERKEL, R.H. (1971): Resistivity analysis for plane-layer half-space models with buried current sources, *Geophys. Prospec.*, **19**, 626-639.

MIZUTANI, H., T. ISHIDO, T. YOKOKURA and S. OHNISHI (1976): Electrokinetic phenomena associated with earthquakes, *Geophys. Res. Lett.*, **3**, 365-368.

NORITOMI, K. (1978): Application of precursory geoelectric and geomagnetic phenomena to earthquake prediction in China, *Chin. Geophys.* (Am. Geophys. Union), **1**, 377-391.

NUR, A. (1972): Dilatancy, pore fluids and premonitory variations of t_s/t_p travel times, *Bull. Seism. Soc. Am.*, **62**, 1217-1222.

PATELLA, D. and A. TRAMACERE (1986): Geoelectric axial dipole sounding curves for a class of two-dimensional earth structures, *Geophys. Prospect.*, **34**, 424-444.

RALEIGH, B., G. BENNET, H. CRAIG, T. HANKS, P. MOLNAR, A. NUR, J. SAVAGE, C. SCHOLZ, R. TURNER and F. WU (1977): Prediction of the Haicheng earthquake, *EOS* (Trans. Am. Geophys. Union), **58**, 236-272.

RIKITAKE, T. (1975): Earthquake precursors, *Bull. Seism. Soc. Am.*, **65**, 1133-1162.

VAROTSOS, P. and K. ALEXOPOULOS (1984a): Physical properties of the variations of the electric field of the earth preceding earthquakes, *Tectonophysics*, **110**, 73-98.

VAROTSOS, P. and K. ALEXOPOULOS (1984b): Physical properties of the variations of the electric field of the earth preceding earthquakes. 2: Determination of epicenter and magnitude, *Tectonophysics*, **110**, 99-125.